

# Denosing of Images for Temperature and Chemiluminescence Measurements of Premixed Flames Applying the Abel Transform

J. C. I. Zamarripa-Ramírez <sup>1,\*</sup>, D. Moreno-Hernández <sup>1,\*</sup> and A. Martinez Gonzalez <sup>2</sup> 

<sup>1</sup> Centro de Investigaciones en Óptica, Loma del Bosque 115, Lomas del Campestre, León 37150, Guanajuato, Mexico

<sup>2</sup> Departamento de Ingeniería Robótica, Universidad Politécnica del Bicentenario, Carr. Silao—Romita Km 2, San Juan de los Duran, Silao 36283, Guanajuato, Mexico; amartinezg@upbcentenario.edu.mx

\* Correspondence: carlos.zamarripa@cio.mx (J.C.I.Z.-R.); dmh@cio.mx (D.M.-H.)

**Abstract:** The temperature field and chemiluminescence measurements of axisymmetric flame are obtained simultaneously in only one image. Digital Laser Speckle Displacement measures temperature fields, and direct image flame determines chemiluminescence values. Applying the Abel transform of axisymmetric objects for volume visualization requires smooth intensity profiles. Due to the nature of the experimental setup, direct image flame is corrupted with speckle noise and a crosstalk effect. These undesirable effects deteriorate the measurement results. Then, experimental data need crosstalk correction and speckle noise reduction to improve the measurements. This work aims to implement a methodology to reduce the speckle noise of highly noisy data intensity profiles to create smooth profiles appropriate to applying the Abel transform. The method uses a Four-Order Partial Differential Equation to reduce speckle noise and a Curve fitting utilizing a set of Gaussian functions to decrease residual undesirable effects. After this, correction of crosstalk is necessary to avoid this effect. The methodology is applied to premixed flames generated with Liquid Petroleum Gas for different mixes.

**Keywords:** chemiluminescence; optics; fluid flow; premixed flames; LPG (Liquid Petroleum Gas)



**Citation:** Zamarripa-Ramírez, J.C.I.; Moreno-Hernández, D.; Martinez Gonzalez, A. Denosing of Images for Temperature and Chemiluminescence Measurements of Premixed Flames Applying the Abel Transform. *Fire* **2023**, *6*, 437. <https://doi.org/10.3390/fire6110437>

Academic Editors: Xuehui Wang, Qinpei Chen and Ali Cemal Benim

Received: 14 September 2023

Revised: 18 October 2023

Accepted: 23 October 2023

Published: 15 November 2023



**Copyright:** © 2023 by the authors. Licensee MDPI, Basel, Switzerland. This article is an open access article distributed under the terms and conditions of the Creative Commons Attribution (CC BY) license (<https://creativecommons.org/licenses/by/4.0/>).

## 1. Introduction

Studying a combustion process is a very complex task [1]. However, the characterization of a flame is essential to improve the combustion process's efficiency and reduce pollutant emissions. Measuring several variables in a flame is used to monitor the efficiency of combustion processes. Generally, some measured variables are flame temperature, soot concentration, radical intensities, flame size, luminosity, and flickering [2–22]. Full-field optical techniques are usually used to make this kind of measurement because they give a global description of the process and do not disturb the sample. On the other hand, simultaneously measuring several variables is preferable because this avoids the lack of correlation between them [9,16–19]. However, a complex optical setup is usually employed for measurement in such cases, making the task costly and challenging [16,18].

The flame equivalence ratio ( $\Phi$ ) is an adimensional variable used to determine if a fuel-oxidizer mixture is rich, lean, or stoichiometric [1]. When  $\Phi > 1$ , it denotes a fuel-rich mixing process; on the other hand,  $\Phi < 1$  is related to fuel-lean mixtures, and the last  $\Phi = 1$  in the ratio relationship is the value for stoichiometric mixing. This relation is intrinsically linked to determining a system's performance. This study, as in others, corroborates that the maximum temperature value is obtained at a value of  $\Phi = 1.05$  for LPG fuel. Other variables that can be connected directly to the flame equivalence ratio are the temperature and radical intensities (chemiluminescence) [10–19]. In a combustion process, some released species are OH, CH, CH<sub>2</sub>O, and C<sub>2</sub>, which have a specific emission spectrum [10–19]. In these combustion flames, the presence of radicals C<sub>2</sub><sup>\*</sup> and CH<sup>\*</sup> are inherent in the reaction zone. These two chemical species are most abundant within

the flame. Furthermore, these radicals emit in the visible region of the electromagnetic spectrum, centered at wavelengths 430 nm and 525 nm, respectively [14]. For this reason, digital color cameras play an essential role in chemiluminescence measurements [11–18]. In this analysis, each color channel contributes specific information about the object under study. However, most digital color cameras suffer from the crosstalk effect; this occurs when sensors have overlapping sensibilities, contaminating the recorded data and needing correction [15,17].

There are few works in which chemiluminescence and flame temperature are measured [3,16–18]. In one of the works, the optical system is simple; they only use a camera, and the temperature is measured using two-color pyrometry. However, temperature measurement is applicable only for sooty flames [3]. In other research, two-color pyrometry is also used to determine the flame's temperature; however, the optical arrangement is complex [16,18]. In [17], the optical configuration is simple to implement, and Digital Laser Speckle Displacement (DLSD) is used to determine the temperature fields. However, the chemiluminescence measurements are contaminated with speckle noise, making determining these values difficult.

On the other hand, in an axisymmetric object, it is well-known that 2D temperature and chemiluminescence values are converted to 3D values through the Abel transforms [17,23–25]. Unfortunately, applying Abel transforms requires noise-free experimental data (smooth experimental curves). Therefore, to achieve proper chemiluminescence measurements in this work, it is necessary to remove the speckle noise to use Abel transforms appropriately. Some studies propose a Fourth-Order Partial Differential Equation (PDE) [26,27]. However, an adverse effect is the elimination of borders on the images and a residual stagger effect impact that creates a blurred image. However, utilizing a Gaussian basis to reconstruct the integrating data image and mitigating the blurring effect is a viable solution [28].

Based on the above, in this work, an image-processing algorithm is applied to recreate the image intensity profile on the object plane by eliminating the speckle effect using a PDE of Fourth Order and a set of Gaussian bases to reconstruct the intensity; furthermore, an Abel transform is applied to the intensity values and a crosstalk correction process is necessary. Therefore, the novelty of this work is to propose an image-processing algorithm to perform the deconvolution of the radiation profiles related to the presence of radicals as CH and C<sub>2</sub>. This has not been performed previously due to the corrupted data derived from speckle phenomena for temperature calculations. This new process implies the possibility of calculating their deconvolution by Abel transform, decreasing the presence of noise by a PDE, and a better profile quality of the radiation from the flame through curve-fitting using a set of Gaussian Bases. In a DLSD system, the temperature values are subject to the refractive index of the gas; then, this approach can be applied to different kinds of flames. In order to calculate the variations in refractive index, correlation algorithms can be used; this limits the number of points from the calculation of temperature profiles and derives in profiles without well-defined borders. In this case, using Gaussian Basis for curve fitting helps increase the number of points and obtain a better representation of temperature calculations numerically. In the setup, no optical filters are needed; the system has low vibration and variable sensitivity. All the data acquisition is made simultaneously so that a relationship between the fuel flow, the temperature, and the chemical emissions can be directly established from the data, circumventing the difficulties that arise when synchronizing two distinct sets of data from two different experimental setups.

## 2. Theoretical Background

### 2.1. Theoretical Development of Intensity Profiles on Flames

When a frame of information is registered on the camera plane, it corresponds to the projected intensity profile of the flame. In some studies of combustion analysis, it is a common topic of interest to determine the reconstructed profile [25]. Therefore, homolog

Abel deconvolution techniques can be used from speckle displacement to intensity. The direct and inverse Abel transforms are linked to analyze the desirable plane:

$$\rho(x, z) = 2 \int_x^\infty \frac{I(r, z) r dr}{\sqrt{r^2 - x^2}} \tag{1}$$

$$I(r, z) = \frac{1}{\pi} \int_r^\infty \frac{\partial \rho(x, z)}{\partial x} \frac{dx}{\sqrt{x^2 - r^2}} \tag{2}$$

where  $\rho(x, z)$  is represented in rectangular reference coordinates and  $(x, z)$  is the profile intensity on the camera plane (see Figure 1). In this work,  $\rho$  can be the chemiluminescence and temperature values. Moreover,  $I(r, z)$  is the original profile intensity of the object in three dimensions in cylindrical coordinates; this is due to the nature of the axisymmetric flames. In this study, the main interest is obtaining the flame’s reconstructed profile intensity  $I(r, z)$ . These profiles are contaminated with speckle phenomena and the crosstalk effect, which makes signal clean-up difficult. However, the procedure presented in this study allows us to obtain appropriate results.

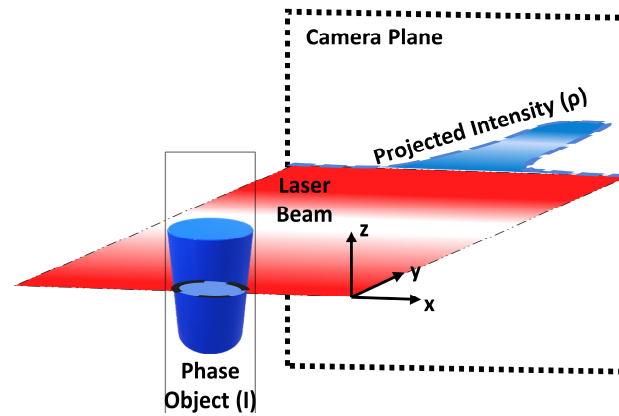


Figure 1. Intensity profile projected on the camera plane from the phase object.

### 2.2. Algorithm for Profile Intensity Noise Reduction

Temperature and chemiluminescence values are obtained using DLSD. The data corresponding to chemiluminescence values require speckle noise reduction. Noise reduction is achieved using a four-order PDE to create a later curve fitting, utilizing a set of Gaussian functions. In the following paragraphs, we expose the three steps of the noise reduction procedure.

1. Elimination of background noise: Firstly, it is necessary to perform a subtraction from the object image minus the reference image:

$$\rho_{(x,z)}^{S_{rgb}} = \rho_{(x,z)}^{O_{rgb}} - \rho_{(x,z)}^{R_{rgb}} \tag{3}$$

In Equation (3), the prefix *S* refers to the subtracted image obtained from the object (*O*) minus the reference image (*R*); the superscript *rgb* means that these are color images and all the channels are involved. In order to reduce the residual speckle presence in the neighborhood of the flame, a median filter is used. Afterward, a simple segmentation is performed to isolate the flame from the background:

$$\rho_{(x,z)}^{S_c} \begin{cases} N & \rho_{(x,z)}^{S_c} \leq t \\ F & \rho_{(x,z)}^{S_c} > t \end{cases} \tag{4}$$

where *N* and *F* are the resultant matrices with the background and flame information, respectively, and the superscript *S<sub>c</sub>* means this operation needs to be applied to each channel independently; here, *t* is found by an iterative method [20].

2. Filter using a four-order (PDE): The residual existence of speckles is characteristic as the median filter is insufficient to eliminate it. Although several algorithms are proposed in the literature for speckle denoising [26,27], this study uses the approach proposed in [26], which implements an algorithm of finite differences to denoise images.

Let the Laplacian of the intensity data be  $\nabla \rho_{i,j}^n$  and the subscripts  $i,j$  be the discretized values of the coordinates  $(x,z)$  from the data obtained on the camera, then:

$$\nabla^2 \rho_{(i,j)}^n = \frac{\rho_{i+1,j}^n + \rho_{i-1,j}^n + \rho_{i,j+1}^n + \rho_{i,j-1}^n - 4\rho_{i,j}^n}{h^2} \tag{5}$$

where the superscript  $n$  means that the target function  $\rho(i,j)$  is calculated by an iterative method, and  $h$  is the stepsize, in the first iteration, a seed value is necessary to obtain the next value on the iteration  $n + 1$ ; therefore, the recursive relation is:

$$\rho_{i,j}^{n+1} = \rho_{i,j}^n - \omega \nabla^2 \rho_{(i,j)}^n \tag{6}$$

where  $\omega$  is a step size linked to the velocity of convergence in the solution, with a suggested value of  $\omega = 0.25$ .

3. Curve fitting by a set of Gaussian bases and deconvolution: Using a finite differences method implies a stagger effect on the pixel values. Therefore, a curve fitment adjustment improves integration performance over the intensity data [28].

$$\rho(x,z) = \sum_{i=1}^k w_i f_i(x,z) \tag{7}$$

where  $\rho(x,z)$  is the profile to adjust for a fixed  $z$ ; in this case, for axisymmetric flames, a set of Gaussian functions can be used appropriately to fit the intensity profiles. Here,  $f_i(x,z) = \exp\left(-\frac{(x-\mu)^2}{2\sigma^2}\right)$ , where  $\mu$  is the mean value of the data from the respective profile, and  $\sigma$  is the standard deviation of the intensity values. Equation (7) can be applied to all the profiles of the image and be represented as a matrix system:

$$\begin{pmatrix} f_1(x_1,z) & f_2(x_1,z) & \dots & f_n(x_1,z) \\ f_1(x_2,z) & f_2(x_2,z) & \dots & f_n(x_2,z) \\ \vdots & \vdots & & \vdots \\ f_1(x_m,z) & f_2(x_m,z) & \dots & f_n(x_m,z) \end{pmatrix} \begin{pmatrix} w_1 \\ w_2 \\ \vdots \\ w_k \end{pmatrix} = \begin{pmatrix} \rho_1 \\ \rho_2 \\ \vdots \\ \rho_m \end{pmatrix} \tag{8}$$

The matrix system in (8) is a system of the type  $Aw = B$ , where  $m$  is the profile position and can be solved by a matrix solution process to obtain the weights.

### 2.3. Abel Reconstruction

After profile noise reduction and curve fitting, 3D Abel transform reconstruction is applied to chemiluminescence and temperature values [17]. Equation (3) is used to fulfill such a purpose. A numerical approximation proposal in N. A. Fomin is used to obtain an approximate reconstruction of the object intensity [24].

### 2.4. Crosstalk Correction

Given the nature of the optical setup to perform temperature and chemiluminescence measurements, the construction of the color camera that uses a Bayer-type filter responsible for the sensibility is more prominent on the green channel than the other two in this device. Therefore, crosstalk correction is needed to obtain the trust intensity values on the object plane. Furthermore, due to the regulation of parameters such as exposure time, saturation,

and others, an approximation of intensity values in the pixels can be proposed in the following way:

$$\hat{I}_i(r, z) = \sum_{i=0}^{k=2} A_{i,j} I_j \quad (9)$$

In this notation, the letter  $I$  means that this correction applies to the reconstructed object intensity profiles. Moreover,  $\hat{I}_i(r, z)$  in the equation is the corrected profile against the crosstalk effect for each RGB color, which means there is a proportionality for each pixel to denote the influence from the overlapped spectral response in the camera, the  $A_{i,j}$  coefficient denotes this; as long as  $I_j$  is the uncorrected intensity registered on the camera sensor; here, the indices ' $i$ ' and ' $j$ ' refer to the color of the illumination source and each pixel, respectively. This equation can be represented in matrix form as follows.

$$\hat{I}_r = A_{r0} I_0 + A_{r1} I_1 + A_{r2} I_2 \quad (10a)$$

$$\hat{I}_g = A_{g0} I_0 + A_{g1} I_1 + A_{g2} I_2 \quad (10b)$$

$$\hat{I}_b = A_{b0} I_0 + A_{b1} I_1 + A_{b2} I_2 \quad (10c)$$

The values of the  $A$  coefficients can be obtained from the camera's graph spectral response. It has been established that certain chemical species are related to efficiency in a combustion process. In this work, two of them are analyzed due to the nature of the premixed flames. These radicals are  $\text{CH}^*$  and  $\text{C}_2^*$ , which emit on the visible region of the electromagnetic spectrum around  $\sim 430$  nm and  $\sim 515$  nm, respectively [14]. Green and blue channels of the color camera are used to measure them. On the other hand, the illumination source, the He-Ne laser, has a wavelength of 633 nm, and is related to calculating temperature profiles related to speckle displacements. Therefore, the effect or red illumination source is depreciated for crosstalk analysis, so subscripts 1 and 2 can be considered for chemiluminescence analysis, substituting them for G and B, respectively; the set of equations [12] can be approximated to a system of two equations with two unknowns.

$$\hat{I}_g \approx A_{gG} I_G + A_{gB} I_B \quad (11a)$$

$$\hat{I}_b \approx A_{bG} I_G + A_{bB} I_B \quad (11b)$$

The previous equations are solved to find the solutions for intensity values from each color channel, as follows:

$$I_G = \frac{A_{bB} \hat{I}_g - A_{gG} \hat{I}_b}{A_{gG} A_{bB} - A_{gB} A_{bG}} \quad (12a)$$

$$I_B = \frac{A_{gBG} \hat{I}_b - A_{bG} \hat{I}_g}{A_{gG} A_{bB} - A_{gB} A_{bG}} \quad (12b)$$

Therefore, the values of intensities  $I_G$  and  $I_B$  correspond to the chemiluminescence measurements.

### 3. Experimental Setup

This work aims to describe a new processing algorithm for the set of images obtained in a previous study from the color spectrum and temperature of an axisymmetric flame [17]. These data were obtained using the optical setup shown in Figure 2. The system consists of a 25 mW He-Ne laser  $\lambda = 638$  nm as the illumination source, and a spatial filter with a microscope objective and a pinhole of  $40\times$  and  $25 \mu\text{m}$ , respectively, a spherical mirror with focal distance  $f = 120$  cm and a diameter  $d = 10$  cm, a butane torch with axisymmetric cylindrical configuration with an inner and outer diameter of 0.5 cm and 1.9 cm, correspondingly, the torch is presented in Figure 2c. Furthermore, to ensure flame temperature control on the head torch, the torch has four slots to admit air into the steam via the Venturi effect. In addition, ground glass of a standard glass of  $12.5 \times 9.5$  cm

and polished 25  $\mu\text{m}$  works as a project surface to generate the speckle phenomena. The last components are a square plane mirror (M2, 6.0  $\times$  6.0 cm), a beam splitter with a transmission rate of 50/50, and the vision system, which is a Lumenera camera model LT225c color digital camera from Lumenera Corporation capable of capturing 170 frames per second in an 8-bit scale of intensity. All the image data are stored in BMP format. The image data were obtained by driving the camera by a semiautomatic subroutine using the manufacturer's software, which allows capturing single or multiple frames. The spectral response of the pixels provided by the manufacturer and used in this work is shown in Figure 3.

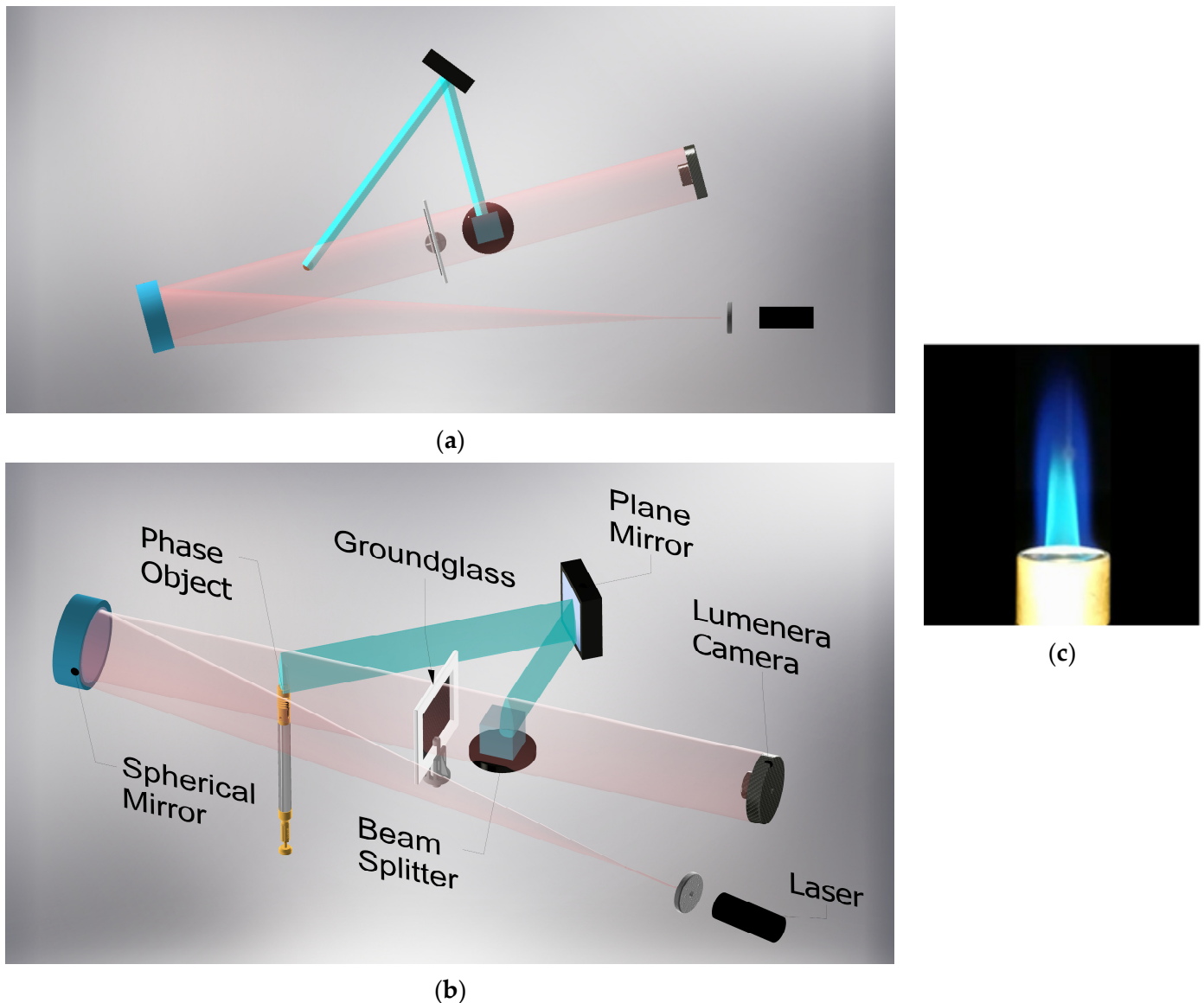


**Figure 2.** (a) Experimental optical setup top view, (b) Isometric view, and (c) Head torch with premixed flame of LPG.

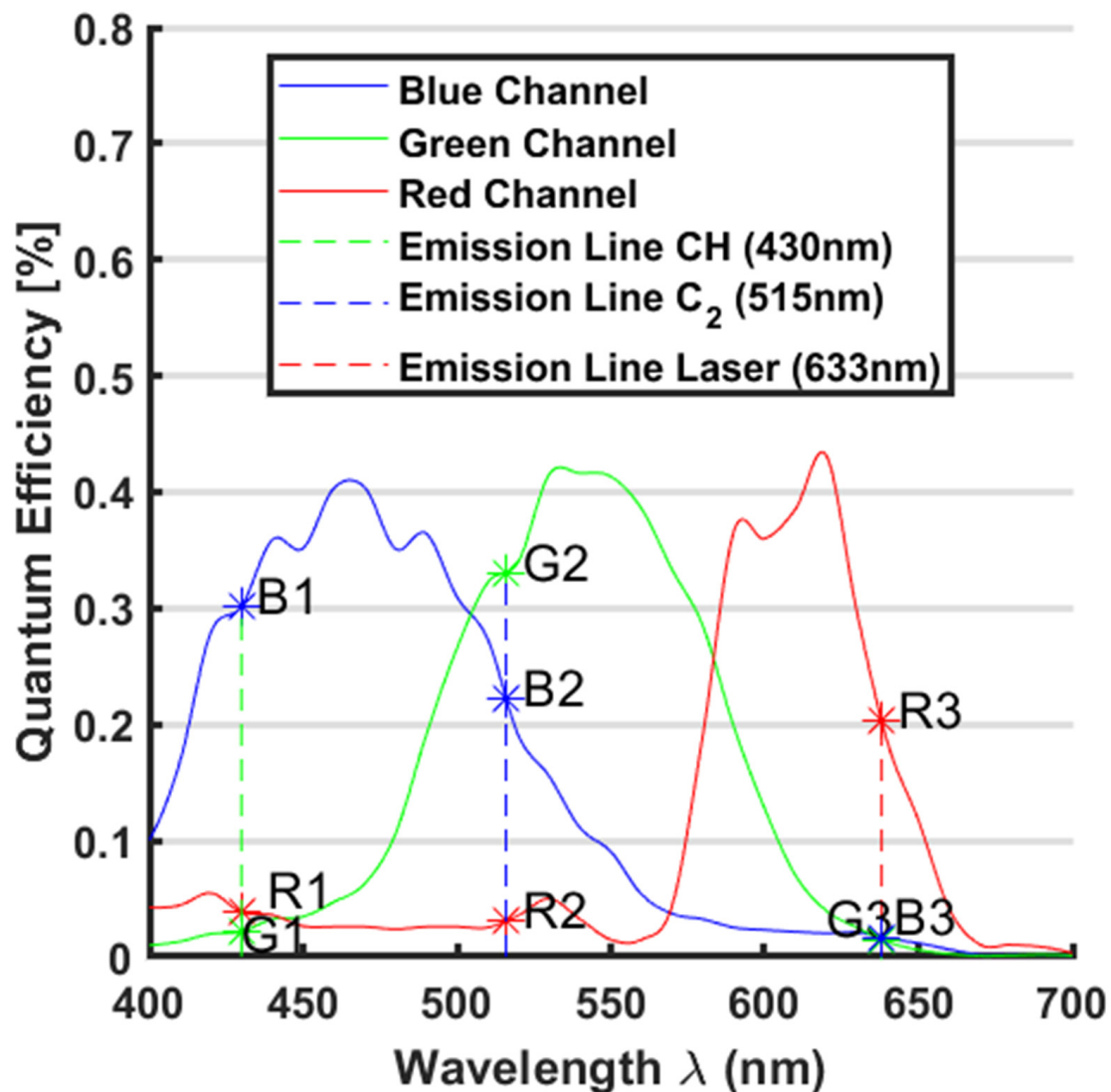
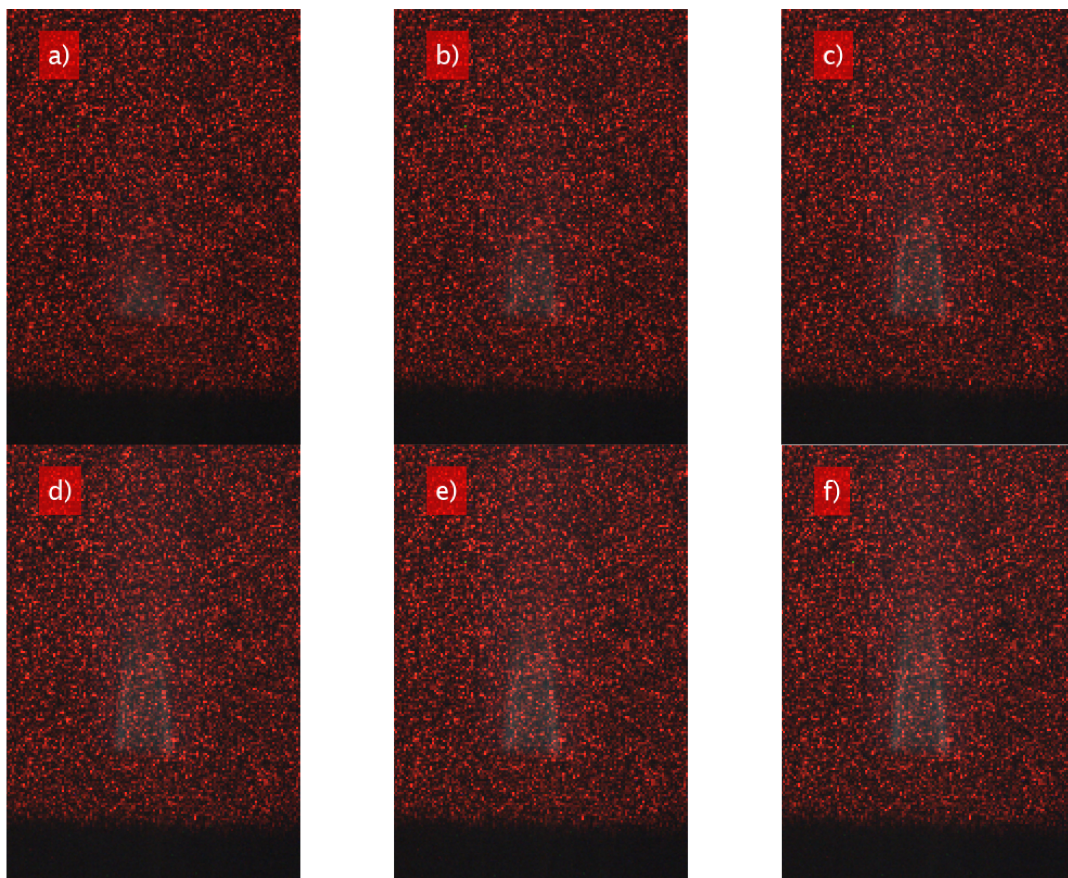


Figure 3. Spectral response from Lumenera Camera [8].

Furthermore, two main paths are used to obtain this data due to the nature of the optical setup and the measurement variables. First, a virtual image of the flame is obtained in the blue path from the plane mirror (M2) and afterward combined on the beam splitter. This trajectory is necessary to measure the chemiluminescence of the flame ( $\text{CH}^*$  and  $\text{C}_2^*$ ). On the other hand, the red path contains all the data from speckle measurements used to calculate the temperature fields. In the experiments, six cases with different fuel ratios were performed using this optical setup; then, the experimental parameters of mixing are concentrated in Table 1; while all the RGB images for each case are present in Figure 4. The figures show a speckled background overlapping with the combination of green and blue color channels that represent the shape of the flame. On the figure can be observed flame size and a residual intensity appearance of the flame, but as was discussed before, a speckle denoising process by applying the procedure presented in Section 2.2 is required to obtain regions of radical presence. The data analysis from radicals and temperatures was performed for all six cases; however, in this work, the results presented in the following are referred to in case f of Figure 4. This discussion is presented in the next section.

**Table 1.** LPG torch experimental conditions.

Equivalence Ratio ( $\Phi$ )	Fuel Flow Rate ( $\text{L}\cdot\text{min}^{-1}$ )		Airflow Rate ( $\text{L}\cdot\text{min}^{-1}$ )
	Propane (70%)	Butane (30%)	
0.95	0.448	0.192	16
1.00	0.476	0.204	16
1.05	0.504	0.216	16
1.11	0.532	0.228	16
1.16	0.560	0.240	16
1.21	0.588	0.252	16

**Figure 4.** Multiple RGB images from combustion cases, (a)  $\Phi = 0.95$ , (b)  $\Phi = 1.00$ , (c)  $\Phi = 1.05$ , (d)  $\Phi = 1.11$ , (e)  $\Phi = 1.16$ , and (f)  $\Phi = 1.21$ .

#### 4. Data Analysis

In this section, a flowchart of the image processing algorithm for chemiluminescence as to temperature analysis is presented in Figure 5. It shows that the algorithm is divided into two sections, one for temperature measurements in the red channel (red box) and the other for the green and blue channel for chemiluminescence analysis (blue-green box). All these processes can be realized with only two frames, a reference frame and a frame in the presence of the phase object (gray box). In the following paragraphs, a detailed description of each step is covered.

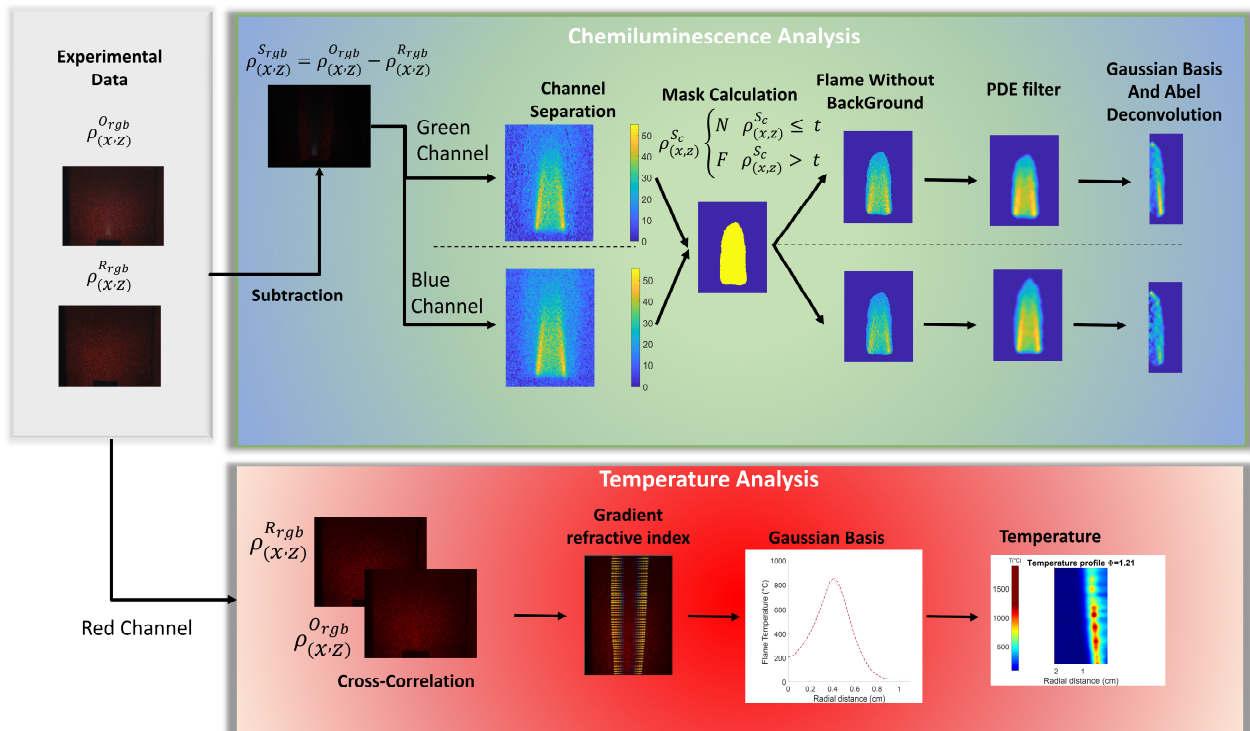


**Figure 5.** Flowchart of the denoising algorithm to calculate the chemiluminescence and temperature profiles for 3D visualization.

All the data analysis presented in this section is for  $\Phi = 1.21$ . As a first step to denoising the signal, the subtraction of the image of the object  $\rho_{(x,z)}^{O_{rgb}}$ , minus the reference image  $\rho_{(x,z)}^{R_{rgb}}$ , is performed. Afterward, the image decomposition on each color channel is performed. Figure 6 presents two profiles with noise from the green and blue channels of the data images for a fixed height taken from the outlet of the head torch. For all this data calculation, the z-axis represents the flame height coordinates (see Figure 1).

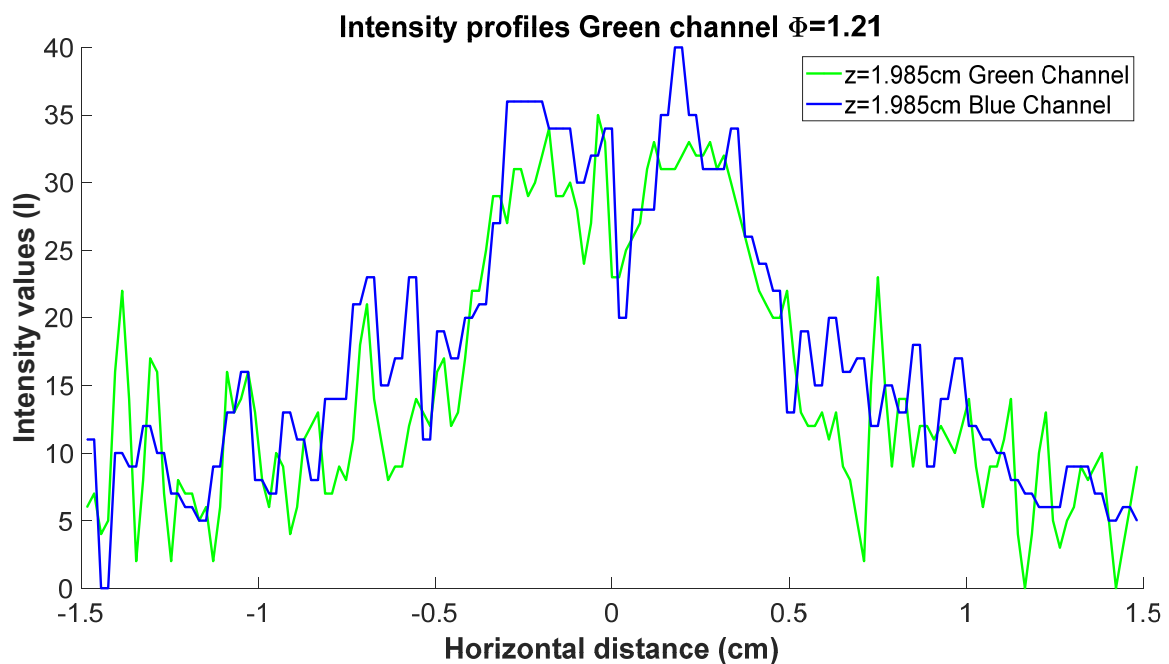
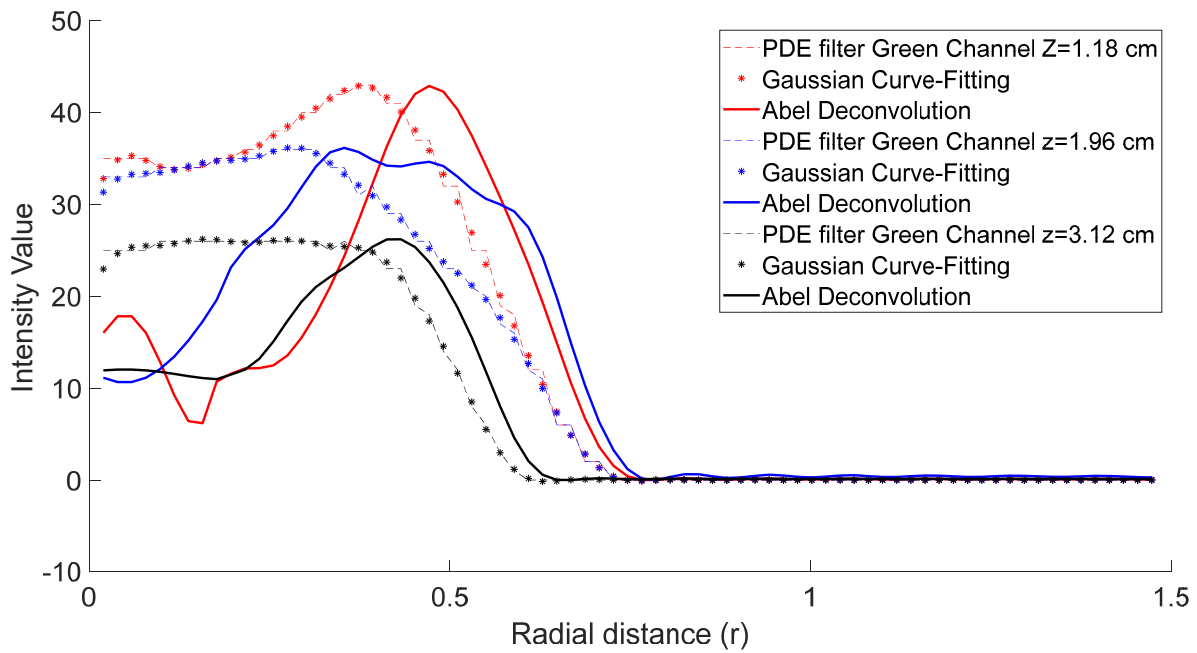


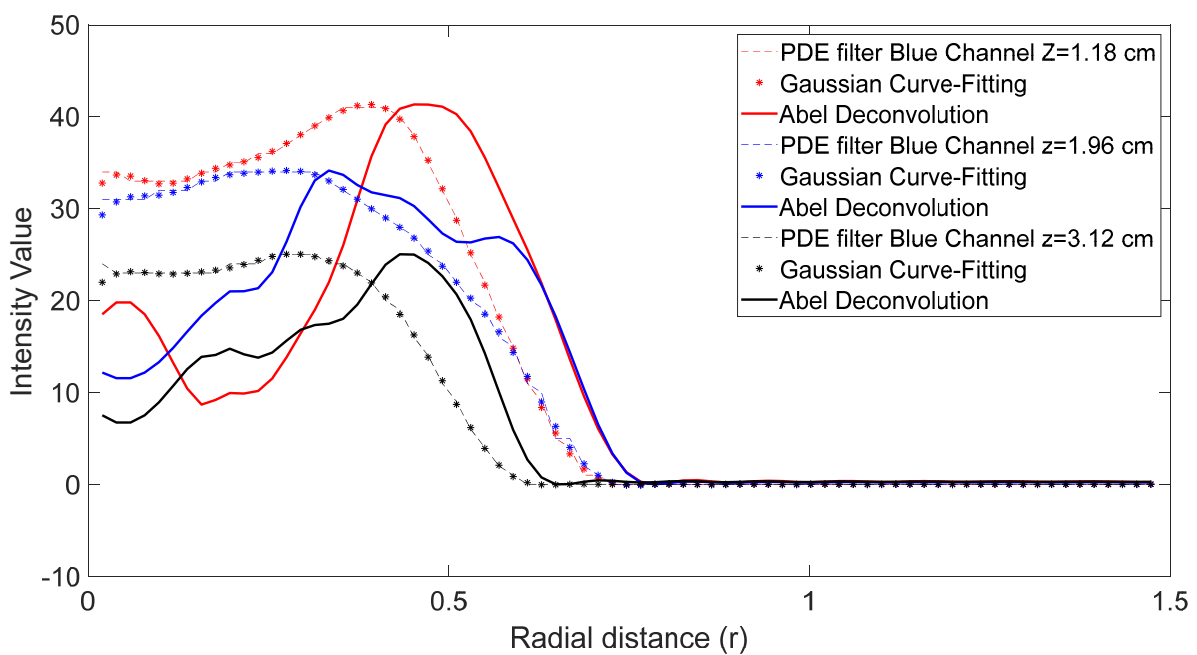
**Figure 6.** Profiles at  $z = 1.985\text{ cm}$  with the presence of speckle noise.

In order to improve the processing time and reduce undesirable data, the original size of images is reduced (see Figure 4). To determine this region, a process to eliminate the background from the flame data is necessary, using the iterative algorithm described in the theoretical background section (see Equation (4)); a subregion of  $151 \times 201$  pixels was determined to contain all the flame intensity information.

In a second instance, speckle denoising was realized to improve the results for numerical integration (Abel transform application). The solution from PDE of fourth order was applied to image intensity data, only blue and green channels. The results are shown in dashed line form in Figure 7a,b for each color channel and three different distances of the z-axis.



(a)



(b)

Figure 7. Cont.

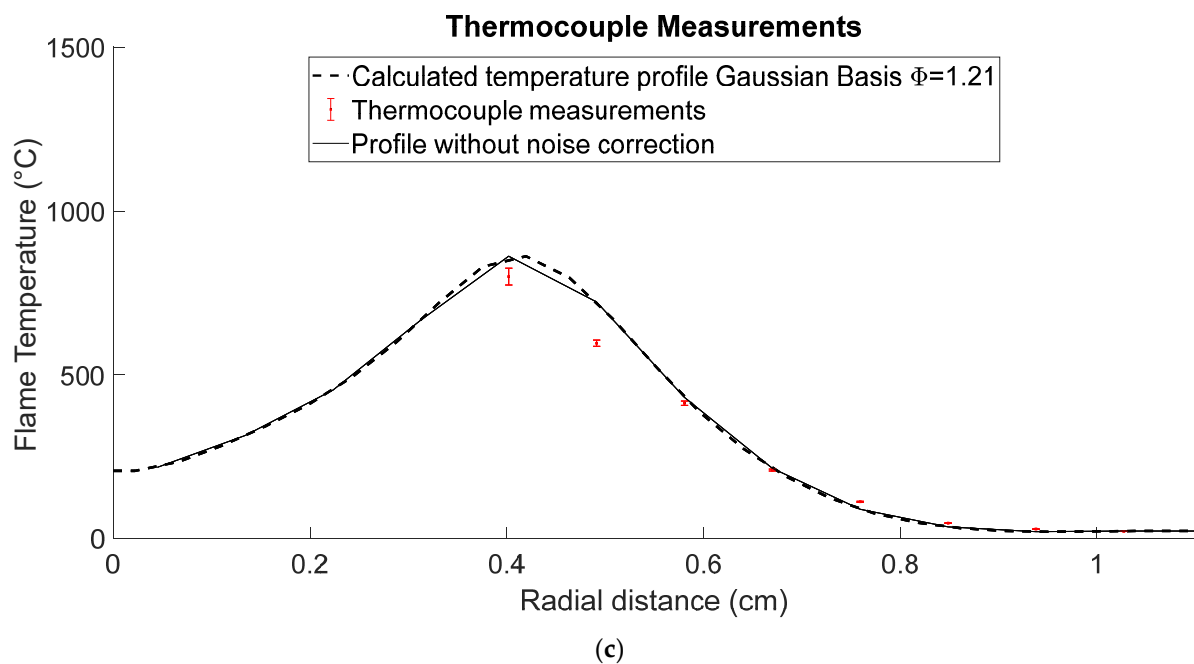


**Figure 7.** Comparative of PDE signal and Gaussian Basis fitting to perform Abel deconvolution (a) Green color channel, (b) Blue color channel, and (c) Temperature profile and thermocouple measurement with error bar calculations.

In Figure 7a,b, the presence of a stagger effect is undeniable; this effect presence is natural due to the discretization process of solving the PDE of intensity by finite differences. However, it can be observed that the speckle effect has disappeared completely, and the borders on image profiles are conserved (dashed line). These profiles were obtained after 40 algorithm iterations to solve the fourth-order PDE. At this point, the intensity profiles are corrected against speckle phenomena. However, the nature of the data can rely on a complicated integrated process due to the stagger effect and discretized values from speckle data. In order to improve the calculation of intensity values by the deconvolution process, a set of Gaussian bases is used to perform the curve fitting of the data. Figure 7a,b in dotted line form represents these curve fittings using the Gaussian basis. It can be observed that the stagger effect has disappeared; the serialized points represent this calculation to obtain the profile in all the values of a specific distance  $r$ , the relative error between the radiation intensity after noise reduction and the measured radiation intensity has a maximum of approximately  $\sim 6\%$  for both channels.

Nevertheless, near the center of the flame, the fitment adjustment process presents a discrepancy; this phenomenon is natural by the proximity of the singularity  $r = 0$ , but it can be interpolated to avoid this problem [24]. The advantage of performing a curve fitment by a set of Gaussian bases is that the borders are prevalent on the image, and a set of well-defined continuous math functions is obtained to define the pixel values of the profiles, which can be used to represent the data on the three-dimensional form using the Abel transform (volume visualization). As a visual aspect, after applying the Abel transform, Figure 7a,b exhibits a difference between the profiles that rely on a clear distinction of regions for concentrations of radicals (continuous line form). Another fact is that this fitment algorithm can be used for temperature calculation from the data obtained by speckle displacements, as shown in Figure 7c. Due to the nature of limited data from correlation algorithms and the use of an interrogation window, the algorithm helps improve the calculation of integration values, eliminating this limitation on data. However, this method can create a synthetic number of points to enhance the estimates of intensity and temperature cases [17]. In the same Figure 7c, a K-type thermocouple was used to corroborate different points' temperature profile measurements. In Figure 7c, the thermocouple measurements consider

the error due to the direct contact between the thermocouple and the flame and exhibit a nonlinear behavior since, near the center of the flame, the error has a value approximately of 3.6% up to a minimum value of 1.5% in areas where the temperature is practically the ambient value. This is represented in the figure with their respective error bars.

As was expected, the results on the lobes with radical concentration are softened, and the mathematic function that describes the profile is calculated. Furthermore, the limited data are avoided by creating any number of calculated points without corruption on the original data. Another critical point is that the fitment curves shown in Figure 7a,b have a mean discrepancy of less than 2% concerning each color channel and a coefficient of correlation of  $R^2 = 0.99$ , which gives certain trust in the calculated values.

In the next step, the crosstalk correction is applied to obtain the intensity values on the object plane. From Figure 3, which has the spectral response of the camera, the  $A$  coefficients using this graph can be determined as  $A_{bB} = 0.3016$ ,  $A_{gB} = 0.0216$ ,  $A_{bG} = 0.2219$  and  $A_{gG} = 0.3322$ . As a result, the system of Equation (12) can be rewritten as:

$$I_B = 3.485\hat{I}_b - 2.34\hat{I}_g \quad (13a)$$

$$I_G = 3.158\hat{I}_b - 0.226\hat{I}_g \quad (13b)$$

This crosstalk correction is applied to each color image (green and blue channel) for every case under analysis. Then, the reconstructed intensity profiles for each color channel for case  $\Phi = 1.21$  are shown in Figure 8a,b; all the intensity values were normalized from zero to one on each color channel. This figure shows the regions with the presence of radicals  $\text{CH}^*$  and  $\text{C}_2^*$ , in Figure 8a, in the interval of height between 2–3.5 cm, approximately the presence of  $\text{CH}^*$  is higher than  $\text{C}_2^*$ , while in Figure 8b, the top of the flame has more appearance of  $\text{C}_2^*$ , which gives a visual result of the presence of these radicals. Another fact to consider is that results exhibit in all the flames a higher proportion of  $\text{C}_2^*$ . These results can be explained as a consequence of the camera construction that uses a Bayer filter, allowing a higher sensibility on this channel. In this study, all the camera settings were configured by default. Additionally, in Figure 8c, the temperature field was obtained using the double amount of data in the Gaussian fitment proposed in this study. Note that the temperature field occupies a larger area than the flame because the convection flow around the flame is also considered in the calculation.

After applying the procedure to reduce the speckle noise and fit the profiles with a set of Gaussian functions to a specific case ( $\Phi = 1.21$ ), we now determine the chemiluminescence values to the other experimental conditions shown in Table 1. Note that the temperature fields are discussed elsewhere [17]. Now, to determine the chemiluminescence values of each case under study (see Table 1), the Lumenera Camera registered a set of 500 images to calculate the average intensities of the reconstructed profiles for the six cases related to the emissions of radicals  $\text{CH}^*$  and  $\text{C}_2^*$  with the new improvement of PDE and gaussian basis, corresponding to green and blue color channels. These intensity values were normalized using the green channel's maximum value. Figure 9 exhibits a linear behavior and a difference between the measurement of noising and denoising data from the green and blue channels, which in turn can improve monitoring of  $\text{CH}^*$  and  $\text{C}_2^*$  at low ratios of the combustion process. Furthermore, the new measurements are from the deconvoluted intensity radiation that represents the three-dimensionality of the flame.

The maximum temperature value calculated for each experimental case is plotted in the same figure. As was expected, the maximum temperature value corresponds to a value of  $\Phi = 1.05$  [1].

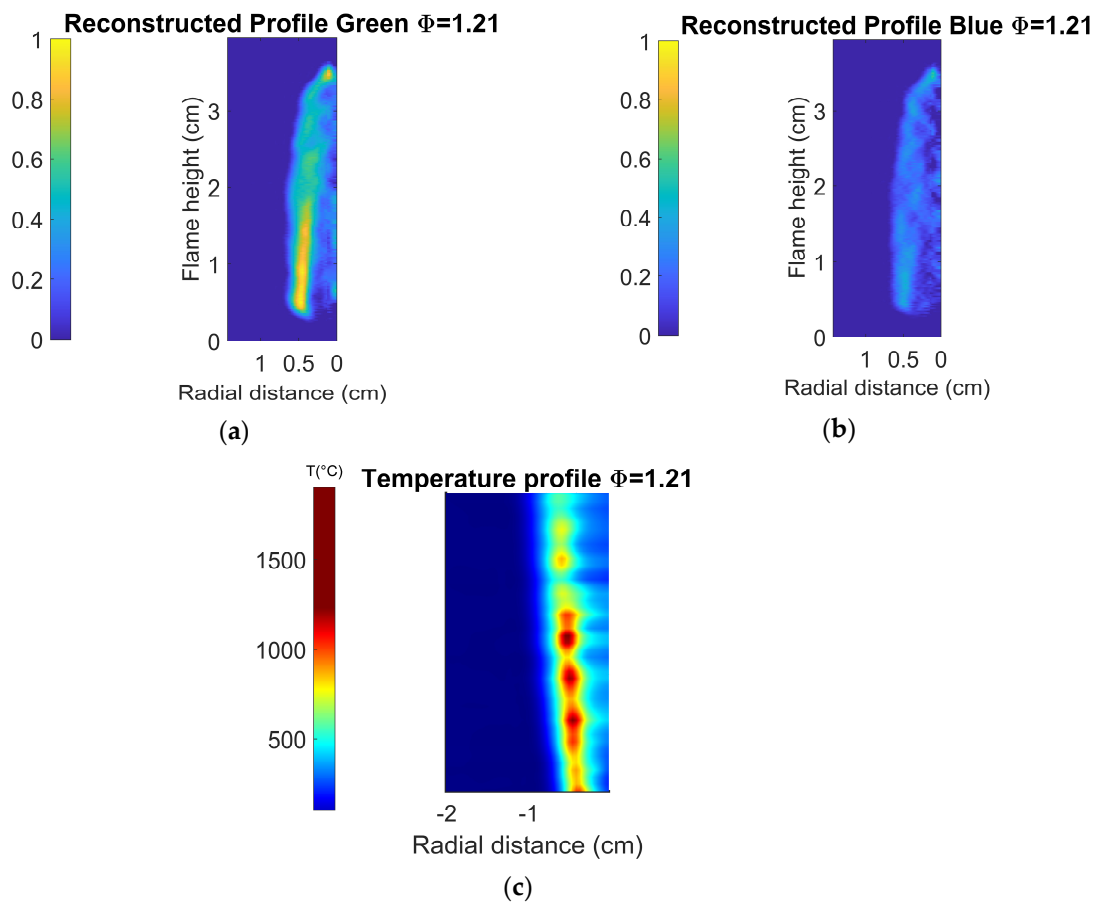


**Figure 8.** Intensity radiation fields with their respective color bar after applying noise reduction, curve fitting, and crosstalk correction (a) Green color channel, (b) Blue color channel, and (c) Temperature field after curve fitting with its respective color bar.

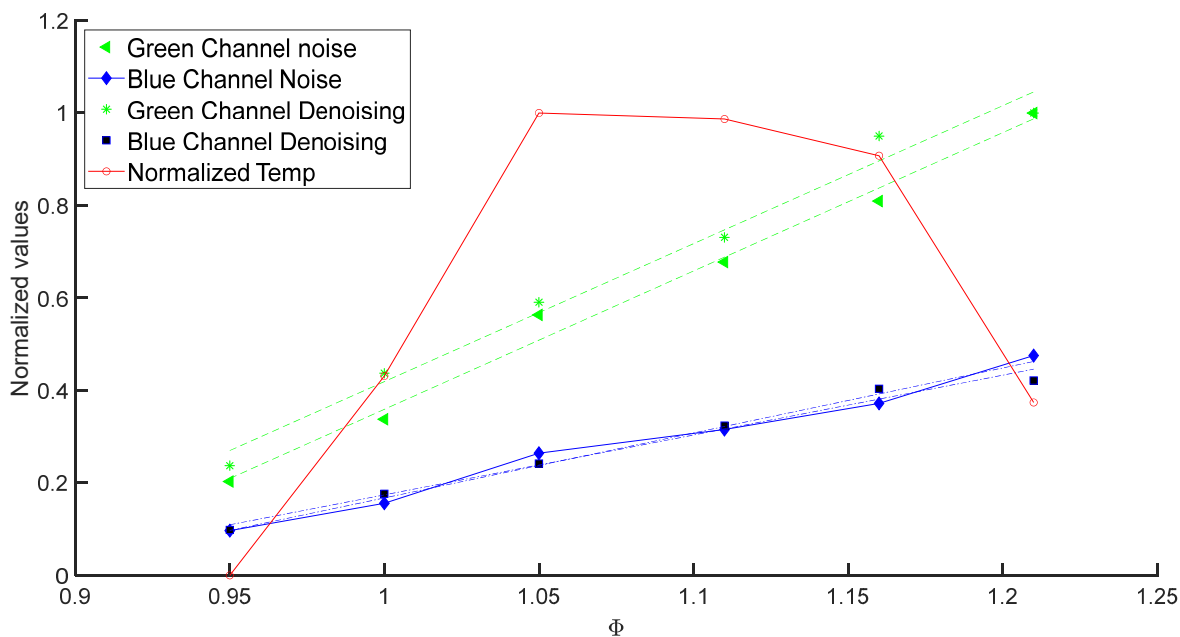


**Figure 9.** Chemiluminescence and the maximum temperature value for each case under study. The chemiluminescence curves exhibit a linear behavior and an increased difference between the quantities at low ratios.

In this way, the approach presented in this work can simplify the monitoring temperature values,  $\text{CH}^*$  and  $\text{C}_2^*$  at low ratios of a combustion process. The linearity fitment of the data has a value of  $R^2 = 0.98$  for each channel and the temperature case has a value of  $R^2 = 0.96$ .

$$ig(\Phi) = 2.9837\Phi - 2.5647 \quad (14a)$$

$$ib(\Phi) = 1.2943\Phi - 1.1202 \quad (14b)$$

$$T(\Phi) = -49.817\Phi^2 + 109.39\Phi - 59.015 \quad (14c)$$

Equation (14a–c) corresponds to a numerical fit of a first- and second-degree numerical function for chemiluminescence and temperature measurements, respectively. The fit was done considering normalized maximum chemiluminescence intensity and temperature.

Finally, this work's optical system can measure temperatures ranging from 100 °C to 1800 °C. Moreover, chemiluminescence detection is of the order of four and forty-two intensity levels approximately. Fixed exposure time and camera gain values are assumed to register all cases studied. The present work is aimed at the study of flames with axial symmetry.

## 5. Conclusions

This work presents an experimental setup to obtain combustion flames' temperature and chemiluminescence measurements in one snapshot. The temperature and chemiluminescence fields are obtained with DLSD and image processing approaches. However, the crosstalk effect and speckle noise contaminate flame radiation images. Crosstalk correction is applied to each green and blue color image. On the other hand, speckle noise present in images is a problem since the Abel transform needs to be applied. Therefore, an image processing algorithm was established in this work to eliminate speckle noise on these data images; the primary purpose is to use a Gaussian basis to avoid singularities and obtain a significant number of points to improve the integration process. The advantage of this process is that very noisy images can reconstruct intensity profiles of flames for three-dimensional visualization to achieve a qualitative and quantitative analysis of regions in radical presence. Furthermore, the simultaneous measurements of temperature and chemiluminescence values ( $\text{CH}^*$  and  $\text{C}_2^*$ ) is a commendable method to monitor the efficiency of combustion processes.

**Author Contributions:** Conceptualization, J.C.I.Z.-R., D.M.-H. and A.M.G.; Methodology, J.C.I.Z.-R., D.M.-H. and A.M.G.; Software, J.C.I.Z.-R.; Formal Analysis, J.C.I.Z.-R. and D.M.-H.; Investigation, J.C.I.Z.-R. and D.M.-H.; Resources, D.M.-H.; Writing-Original draft, J.C.I.Z.-R. and D.M.-H. All authors have read and agreed to the published version of the manuscript.

**Funding:** This research received no external funding.

**Institutional Review Board Statement:** Not applicable.

**Informed Consent Statement:** Not applicable.

**Data Availability Statement:** Data underlying the results presented in this article are not publicly available but may be available from the corresponding authors upon reasonable request.

**Acknowledgments:** The authors gratefully acknowledge (CONACYT) through different projects.

**Conflicts of Interest:** The authors declare that there is no conflict of interest related to this article.

## References

1. Günther, R. *Flames—Their Structure, Radiation and Temperature*. Von A. G. Gaydon und H. G. Wolfhard. Chapman and Hall Ltd., London 1979 4. Aulf., XIII, 449 S., zahlr. Abb. u. Tab., Ln., £18.00. *Chem. Ing. Tech.* **1979**, *51*, 765. [[CrossRef](#)]
2. Zhou, Y.; Zheng, D. Study on Measurement of Flame Temperature Using a Linear CCD. In *Proceedings of the International Technology and Innovation Conference 2006 (ITIC 2006)*, London, UK, 11–12 October 2006; IEEE: Hangzhou, China, 2006; Volume 2006, pp. 1647–1650. [[CrossRef](#)]

3. Toro, N.C.; Arias, P.L.; Torres, S.; Sbarbaro, D. Flame Spectra-Temperature Estimation Based on a Color Imaging Camera and a Spectral Reconstruction Technique. *Appl. Opt.* **2014**, *53*, 6351. [[CrossRef](#)] [[PubMed](#)]
4. Zhao, H.; Feng, H.; Xu, Z.; Li, Q. Research on Temperature Distribution of Combustion Flames Based on High Dynamic Range Imaging. *Opt. Laser Technol.* **2007**, *39*, 1351–1359. [[CrossRef](#)]
5. Alvarez-Herrera, C.; Moreno-Hernández, D.; Barrientos-García, B. Temperature Measurement of an Axisymmetric Flame by Using a Schlieren System. *J. Opt. A Pure Appl. Opt.* **2008**, *10*, 104014. [[CrossRef](#)]
6. Farrell, P.V.; Hofeldt, D.L. Temperature Measurement in Gases Using Speckle Photography. *Appl. Opt.* **1984**, *23*, 1055. [[CrossRef](#)] [[PubMed](#)]
7. Fujisawa, N.; Aiura, S.; Ohkubo, M.; Shimizu, T. Temperature Measurement of Dilute Hydrogen Flame by Digital Laser-Speckle Technique. *J. Vis.* **2009**, *12*, 57–64. [[CrossRef](#)]
8. Wang, Y.; Chung, S.H. Soot Formation in Laminar Counterflow Flames. *Prog. Energy Combust. Sci.* **2019**, *74*, 152–238. [[CrossRef](#)]
9. Legros, G.; Wang, Q.; Bonnet, J.; Kashif, M.; Morin, C.; Consalvi, J.-L.; Liu, F. Simultaneous Soot Temperature and Volume Fraction Measurements in Axis-Symmetric Flames by a Two-Dimensional Modulated Absorption/Emission Technique. *Combust. Flame* **2015**, *162*, 2705–2719. [[CrossRef](#)]
10. Hardalupas, Y.; Orain, M.S.; Panoutsos, C.; Taylor, A.M.K.P.; Olofsson, J.; Seyfried, H.; Richter, M.; Hult, J.; Aldén, M.; Hermann, F.; et al. Chemiluminescence Sensor for Local Equivalence Ratio of Reacting Mixtures of Fuel and Air (FLAMESEEK). *Appl. Therm. Eng.* **2004**, *24*, 1619–1632. [[CrossRef](#)]
11. Kojima, J.; Ikeda, Y.; Nakajima, T. Basic Aspects of OH(A), CH(A), and C<sub>2</sub>(d) Chemiluminescence in the Reaction Zone of Laminar Methane–Air Premixed Flames. *Combust. Flame* **2005**, *140*, 34–45. [[CrossRef](#)]
12. Huang, H.-W.; Zhang, Y. Flame Colour Characterization in the Visible and Infrared Spectrum Using a Digital Camera and Image Processing. *Meas. Sci. Technol.* **2008**, *19*, 085406. [[CrossRef](#)]
13. Huang, H.W.; Zhang, Y. Digital Colour Image Processing Based Measurement of Premixed CH<sub>4</sub>+air and C<sub>2</sub>H<sub>4</sub>+air Flame Chemiluminescence. *Fuel* **2011**, *90*, 48–53. [[CrossRef](#)]
14. Trindade, T.; Ferreira, A.; Fernandes, E. Characterization of Combustion Chemiluminescence: An Image Processing Approach. *Procedia Technol.* **2014**, *17*, 194–201. [[CrossRef](#)]
15. Yang, J.; Ma, Z.; Zhang, Y. Improved Colour-Modelled CH\* and C<sub>2</sub>\* Measurement Using a Digital Colour Camera. *Measurement* **2019**, *141*, 235–240. [[CrossRef](#)]
16. Cai, W.; Kaminski, C.F. A Tomographic Technique for the Simultaneous Imaging of Temperature, Chemical Species, and Pressure in Reactive Flows Using Absorption Spectroscopy with Frequency-Agile Lasers. *Appl. Phys. Lett.* **2014**, *104*, 034101. [[CrossRef](#)]
17. Zamarripa-Ramírez, J.C.I.; Moreno-Hernández, D.; Martínez-González, A. Simultaneous Measurement of Temperature and Color Spectrum of Axisymmetric Premixed Flames Using Digital Laser Speckle Photography and an Image Processing Approach. *Meas. Sci. Technol.* **2021**, *32*, 105903. [[CrossRef](#)]
18. Chorey, D.; Jagadale, V.; Prakash, M.; Hanstorp, D.; Andersson, M.; Deshmukh, D.; Mishra, Y.N. Simultaneous Imaging of CH\*, C<sub>2</sub>\*, and Temperature in Flames Using a DSLR Camera and Structured Illumination. *Appl. Opt.* **2023**, *62*, 3737. [[CrossRef](#)]
19. Hardalupas, Y.; Orain, M. Local Measurements of the Time-Dependent Heat Release Rate and Equivalence Ratio Using Chemiluminescent Emission from a Flame. *Combust. Flame* **2004**, *139*, 188–207. [[CrossRef](#)]
20. Lundberg, J.; Henriksen, M.; Gaathaug, A. Using Image Processing for Flame Diagnostics. In *Linköping Electronic Conference Proceedings, Proceedings of the 58th Conference on Simulation and Modelling (SIMS 58) Reykjavik, Iceland, 25–27 September 2017*; Linköping University Electronic Press: Linköping, Sweden, 2017; pp. 168–173. [[CrossRef](#)]
21. Al-Tayyar, M.A.; AlKhafaji, D.; Shahad, H.A. A Review on Flame Height and Structure and Pollutants Formation. *Neuro Quantology* **2022**, *20*, 2946–2968. [[CrossRef](#)]
22. Tanoue, K.; Ogura, Y.; Takayanagi, M.; Nishimura, T. Measurement of Temperature Distribution for the Flickering Phenomenon around the Premixed Flame by Using Laser Speckle Method. *J. Vis.* **2010**, *13*, 183–185. [[CrossRef](#)]
23. Buie, M.J.; Pender, J.T.P.; Holloway, J.P.; Vincent, T.; Ventzek, P.L.G.; Brake, M.L. Abel's Inversion Applied to Experimental Spectroscopic Data with off Axis Peaks. *J. Quant. Spectrosc. Radiat. Transf.* **1996**, *55*, 231–243. [[CrossRef](#)]
24. Fomin, N.A. *Speckle Photography for Fluid Mechanics Measurements*; Springer: Berlin/Heidelberg, Germany, 1998. [[CrossRef](#)]
25. Dreyer, J.A.H.; Slavchov, R.I.; Rees, E.J.; Akroyd, J.; Salamanca, M.; Mosbach, S.; Kraft, M. Improved Methodology for Performing the Inverse Abel Transform of Flame Images for Color Ratio Pyrometry. *Appl. Opt.* **2019**, *58*, 2662. [[CrossRef](#)]
26. You, Y.-L.; Kaveh, M. Fourth-Order Partial Differential Equations for Noise Removal. *IEEE Trans. Image Process* **2000**, *9*, 1723–1730. [[CrossRef](#)]
27. Rudin, L.I.; Osher, S.; Fatemi, E. Nonlinear Total Variation Based Noise Removal Algorithms. *Phys. D Nonlinear Phenom.* **1992**, *60*, 259–268. [[CrossRef](#)]
28. Rosa-Miranda, E.D.L.; Berriel-Valdos, L.R.; Gonzalez-Ramirez, E.; Alaniz-Lumbreras, D.; Saucedo-Anaya, T.; De La Rosa-Vargas, J.I.; Villa-Hernandez, J.J.; Torres-Arguelles, V.; Castano, V.M. An Alternative Approach to the Tomographic Reconstruction of Smooth Refractive Index Distributions. *J. Eur. Opt. Soc.-Rapid Publ.* **2013**, *8*, 13036. [[CrossRef](#)]

**Disclaimer/Publisher's Note:** The statements, opinions and data contained in all publications are solely those of the individual author(s) and contributor(s) and not of MDPI and/or the editor(s). MDPI and/or the editor(s) disclaim responsibility for any injury to people or property resulting from any ideas, methods, instructions or products referred to in the content.